

HIP-MWT – A NEW CELL CONCEPT FOR INDUSTRIAL PROCESSING OF HIGH-PERFORMANCE METAL WRAP THROUGH SILICON SOLAR CELLS

B. Thaidigsmann¹, A. Spribille¹, H. Plagwitz², G. Schubert², F. Fertig¹, F. Clement¹, A. Wolf¹, D. Biro¹, R. Preu¹

¹Fraunhofer Institute for Solar Energy Systems ISE, Heidenhofstr. 2, D-79110 Freiburg, Germany

²Sunways AG Photovoltaic Technology, Macairestraße 3, D-78467 Konstanz, Germany

Phone: +49 761 4588 5563, email: benjamin.thaidigsmann@ise.fraunhofer.de

ABSTRACT:

This work presents recent progress in research on multicrystalline silicon solar cells based on the HIP-MWT concept, a simplified structure for high-performance metal wrap through cells with rear surface passivation. With the simplified approach, no structured rear emitter is required as the rear dielectric acts as an insulating layer to isolate the n-type contacts from the p-type base. The fabricated large-area HIP-MWT solar cells with Al₂O₃ rear surface passivation and screen-printed contacts show conversion efficiencies of up to 18.2 % (confirmed) and clearly outperform both H-pattern PERC and MWT-BSF reference cells in terms of efficiency. The reverse bias behaviour of the cells is investigated using dark lock-in thermography and reverse current-voltage data.

Keywords: MWT, PERC, MIS, reverse bias

1 INTRODUCTION

The interest in metal wrap through (MWT) technology [1] increased strongly over the past years. The MWT approach improves the short circuit current of the cells and allows for novel module concepts [2]. A way to further increase cell efficiency is the integration of a passivated rear surface resulting in an MWT-PERC structure (metal wrap through passivated emitter and rear cell) [3,4]. With regard to conversion efficiency, this combined structure shows a remarkable potential. In recent experiments conversion efficiencies exceeding 20 % have been demonstrated for large area Cz-Si MWT-PERC-type cells [5]. However, process complexity increases due to several additional features. The HIP-MWT approach (high-performance metal wrap through) [6] addresses this issue by replacing the emitter beneath the rear n-type metallization by a dielectric insulating layer as shown in Figure 1. This permits the application

of a full area diffusion barrier on the rear side and thus reduces the effort for the integration of the MWT concept into typical process sequences for PERC-type cells to a minimum. This allows for much easier and more economical industrial processing compared to previous MWT-PERC approaches.

Within this work mc-Si MWT cells with aluminium back surface field (MWT-BSF), conventional passivated emitter and rear cells (PERC) with H-pattern front grid, non-simplified MWT-PERC-type cells and HIP-MWT cells are fabricated. This allows for a rating of the different approaches and a direct comparison of the HIP-MWT concept to the non-simplified MWT-PERC structure.

2 APPROACH

All process steps are carried out in the pilot line PV-TEC [7]. Figure 2 displays the process sequence for the fabrication of the presented HIP-MWT solar cells. 200 µm thick multicrystalline silicon wafers with an edge length of 156 mm and a base resistivity of ~2 Ωcm are textured in an acidic inline texturing system. Rear side

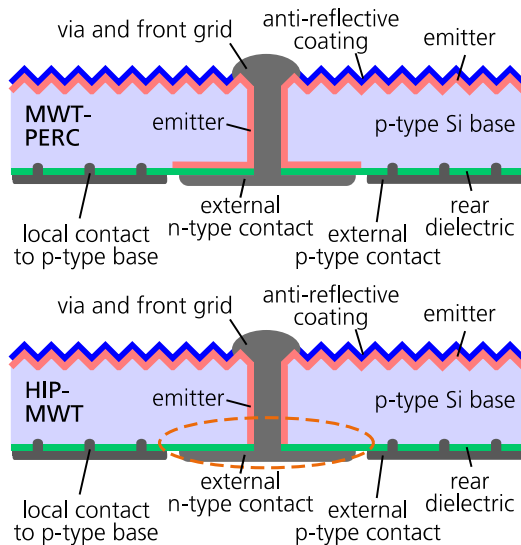


Figure 1: Comparison of the non-simplified MWT-PERC structure and the simplified HIP-MWT structure. The HIP-MWT structure does not feature an emitter underneath the rear n-type contact (dashed oval). Instead, the rear passivation layer stack synergistically provides insulation between n-type contact and p-type base.



Figure 2: Process sequence for the fabrication of the presented mc-Si HIP-MWT solar cells. Laser drilling of vias (dashed border) forms the only additional process step compared to a typical PERC-type process sequence.

polishing enhances light trapping and passivation quality in the finished cell. A SiO_x diffusion barrier deposited by plasma enhanced chemical vapour deposition (PECVD) prevents emitter formation on the rear side. With an adapted pre-cleaning step prior to diffusion, laser drilling of the vias is the only additional process step needed for the integration of the MWT concept compared to a typical process sequence for H-pattern PERC-type cells. We use plasma enhanced chemical vapour deposition for the formation of the Al_2O_3 -based rear side passivation stack and the SiN_x anti-reflective coating. The deposited rear dielectric ensures proper insulation between external n-type contact and p-type base (see Figure 1) and supersedes emitter formation on the rear surface. Therefore no structuring steps for the rear diffusion barrier are necessary. Screen printing of the metal contacts including soldering pads ensures industrial feasibility. After contact firing a laser locally alloys the rear aluminium through the dielectric passivation layer stack by means of the laser fired contact technology (LFC) [8]. A forming gas anneal is performed in a walking string furnace with high throughput [9].

The reference MWT cells with aluminium back surface field are produced in a separate batch on comparable material using our standard MWT-BSF process sequence [10]. PERC-type reference cells are produced in parallel to the HIP-MWT cells omitting laser drilling and adapting the metallization layout. For the non-simplified MWT-PERC-type reference cells, the rear diffusion barrier is structured using screen-printed etch resist and subsequent etching in buffered HF.

3 RESULTS

3.1 Current voltage characteristics

Table I shows current-voltage data for the different cell types measured with an industrial cell tester. MWT, PERC, non-simplified MWT-PERC reference cells and three groups of HIP-MWT cells are displayed (HIP-

Table I: Current-voltage data of the devices produced in this work. Cell thickness is 180 μm after processing, edge length is 156 mm. The numbers in brackets next to “median” indicate the number of cells in each group. Cell efficiencies are measured directly after processing with an industrial cell tester. For HIP-MWT, various rear dielectrics have been investigated (HIP-MWT I, II, III). The material used for group HIP-MWT III differs from the other groups.

Device group	Category	V_{OC} (mV)	J_{SC} (mA/cm^2)	FF (%)	$p\text{FF}$ (%)	η (%)
MWT-BSF	median (5)	610	34.8	77.6	80.5	16.5
	<i>best cell</i>	610	34.9	77.7	80.5	16.5
PERC	median (4)	627	35.3	76.6	81.4	17.0
	<i>best cell</i>	632	35.9	76.2	81.7	17.3
MWT-PERC	median (9)	627	36.7	75.8	81.1	17.3
	<i>best cell</i>	632	37.2	76.1	81.5	17.9
HIP-MWT I	median (8)	629	36.7	75.7	81.3	17.5
	<i>best cell</i>	632	37.2	75.8	81.4	17.8
HIP-MWT II	median (6)	632	37.0	75.7	81.4	17.6
	<i>best cell</i>	634	37.2	75.8	81.5	17.9
HIP-MWT III	median (29)	631	37.0	76.9	81.3	18.0
	<i>best cell</i>	637	37.1	77.3	81.7	18.3
	<i>best cell</i>	637	36.9	77.3		18.2*

*measurement by Fraunhofer ISE CaLab

MWT I to III). All groups except “HIP-MWT III” are fabricated on material from the same manufacturer. The numbers “I” to “III” indicate different rear dielectrics used for the HIP-MWT cells.

The data reveals a clear advantage for cells with a passivated rear surface. An increase in cell efficiency of $\sim 1\%_{\text{abs}}$ is visible for the MWT-PERC and HIP-MWT structures in comparison to MWT-BSF cells caused by an increase in both open circuit voltage V_{OC} and short circuit current J_{SC} . With the metal wrap through concept, shading of the front side decreases from $\sim 7\%$ to $\sim 4\%$ resulting in an increase in short circuit current density of $\sim 1.3\text{ mA}/\text{cm}^2$.

The groups MWT-PERC and HIP-MWT I are processed in parallel and show an equal composition of the rear side passivation and metallization. The sole difference is the rear emitter underneath the n-type contact that is only present for the non-simplified MWT-PERC cells (see Figure 1). No significant difference in the current-voltage data is visible in a direct comparison of both structures, confirming the feasibility of the simplified HIP-MWT structure. Especially the pseudo fill factor, which decreases for shunt-like loss mechanisms, is equal for both concepts. Compared to PERC-type cells the conversion efficiency increases by $\sim 0.5\%_{\text{abs}}$ for the HIP-MWT I cells. This increase is achieved by a single additional process step – the drilling of vias – and an adapted low-cost pre-cleaning step prior to diffusion.

With an increased thickness of the rear dielectric, an impressive median short circuit current density of $J_{\text{SC}} = 37.0\text{ mA}/\text{cm}^2$ and a median open circuit voltage of $V_{\text{OC}} = 632\text{ mV}$ is reached resulting in a median conversion efficiency of 17.6 % for group HIP-MWT II. Group HIP-MWT III is fabricated using an enhanced rear side passivation layer stack that allows for improved LFC formation and increases reverse stability of the cells (see section 3.3). The cells are fabricated from different mc-Si material with an optimized metallization and LFC layout and reach an impressive median conversion efficiency of $\eta = 18.0\%$ (29 cells), mainly due to an increased fill factor.

3.2 Short circuit current analysis

With both approaches, MWT and PERC, losses in short circuit current are reduced. Combined structures such as MWT-PERC and HIP-MWT therefore yield the highest J_{SC} values (see Table I). Table II shows the

Table II: Estimated J_{SC} loss due to the relevant loss mechanisms. The values indicate the possible improvement in J_{SC} that is achievable by eliminating each individual loss mechanism. The values in column “ ΔJ_{SC} ref” refer to a simulation without shading, ideal light trapping (no escape reflectance, no parasitic absorption at the rear surface) and no rear surface recombination. Values for conventional H-pattern BSF cells are given for the sake of completeness.

Device group	shading	escape reflectance	parasitic absorption	S_{eff} rear	ΔJ_{SC} ref
BSF	7 %	0.5 %	3.5 %	2 %	16 %
MWT-BSF	4 %	0.5 %	3.5 %	2 %	12 %
PERC	7 %	1 %	1.5 %	0.5 %	12 %
HIP-MWT I	4 %	1 %	1.5 %	0.5 %	8 %

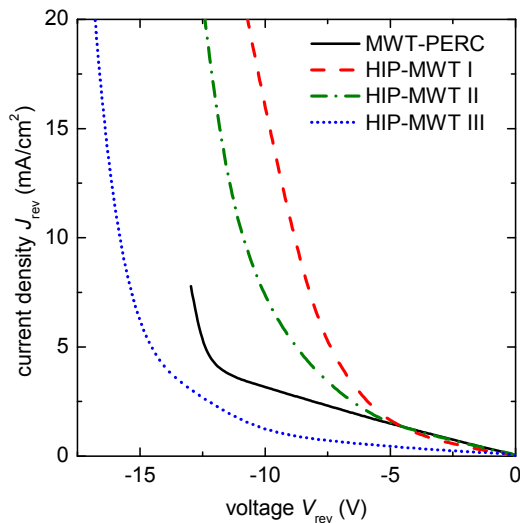


Figure 3: Comparison of dark current-voltage characteristics for a MWT-PERC reference cell and HIP-MWT cells with different rear dielectrics.

possible improvements in J_{SC} for different cell structures and relevant loss mechanisms. The values are calculated with PC1D simulations [11] based on IQE and reflectance data. An effective rear surface recombination velocity of 500 cm/s for Al-BSF and 100 cm/s for the PERC-type rear side are assumed whereas the rear surface reflectance is set to 75 % (diffuse) and 93 % (specular) respectively.

As the different loss mechanisms interact, a summation of the individual contributions is not possible. Instead, a reference simulation where all specified loss mechanisms are deactivated serves as a reference and yields a maximum current density of $J_{SC} = 40 \text{ mA/cm}^2$ – bulk and emitter recombination as well as front reflectance are still active in this simulation. Compared to this reference value, HIP-MWT cells show the lowest loss in short circuit current. A theoretical improvement of ~16 % is expected for conventional H-pattern BSF solar cells when ideal rear surface passivation and no internal optical losses such as escape reflectance and parasitic absorption at the rear surface are assumed. For HIP-MWT cells, this value decreases to only 8 % or 3 mA/cm^2 , which demonstrates the high potential of MWT-PERC-like structures in reducing J_{SC} losses.

3.3 Reverse current voltage characteristics

Partial shading of a photovoltaic module may result in reverse bias conditions for the shaded cells. The maximum reverse voltage in such a configuration depends on the length of the individual strings that are secured by a bypass diode. A typical voltage for reverse bias stability testing is $V_{rev} = -12 \text{ V}$.

Table III: Median values for shunt resistance R_p , dark current density J_{rev1} at $V_{rev1} = -1 \text{ V}$ and current density J_{rev2} at $V_{rev2} = -12 \text{ V}$.

Device group	R_p (k Ω)	J_{rev1} (mA/cm 2)	J_{rev2} (mA/cm 2)
PERC	7.8	0.2	4.4
MWT-PERC	3.6	0.4	6.6
HIP-MWT I	6.5	0.2	29.8
HIP-MWT II	5.0	0.3	18.5
HIP-MWT III	11.7	0.2	3.3

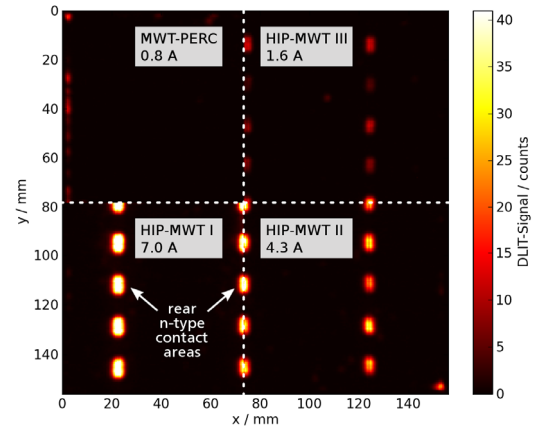


Figure 4: Spatially resolved DLIT signal (detail) for selected HIP-MWT and MWT-PERC cells with different rear dielectrics obtained at a reverse bias of -10 V. The signal is proportional to the local heat dissipation and thus correlates with the local current density. The overall reverse current is indicated below the device group. An increase of the signal is visible underneath the rear external n-type contacts.

Due to the fact that the rear n-type contact overlaps the p-type base, the rear dielectric of HIP-MWT cells must provide reliable insulation between both polarities especially under reverse bias. Previous experiments revealed a junction breakdown underneath the rear n-type contact at voltages below -6 V for a rear dielectric consisting of Al_2O_3 and SiN_x [12]. As shown in Figure 3, the presented cells of group HIP-MWT I show a similar behaviour for voltages below -6 V. The thickness of the rear SiN_x capping layer is increased for the cells of group HIP-MWT II resulting in a slightly lower current flow and therefore improved reverse bias stability. Nevertheless, the median current J_{rev2} at $V_{rev} = -12 \text{ V}$ still exceeds the value of the MWT-PERC reference cells (see Table III). In contrast, the enhanced rear dielectric layer stack of group HIP-MWT III deposited by PECVD allows for median J_{rev2} values of only 3.3 mA/cm^2 . This is even less than for the non-simplified MWT-PERC reference cells and enables conventional module assembly. Within the group of 29 processed HIP-MWT III cells, a maximum value of only 6.0 mA/cm^2 is measured for J_{rev2} , confirming the reliability and stability of this concept.

3.4 Spatial distribution of the current under reverse bias

Apart from the overall current, the spatial distribution of the current flow under reverse bias conditions is crucial for preventing hot spots. Figure 4 shows dark lock-in thermography (DLIT) [13] mappings recorded at $V_{rev} = -10 \text{ V}$ for MWT-PERC reference cells and the presented HIP-MWT cells with varying rear dielectric.

An increase in current density underneath the rear n-type contact is visible for all HIP-MWT cells. While conventional cells show a rather unpredictable current distribution, the current of HIP-MWT cells under reverse bias almost explicitly flows in a pre-defined region – the rear local n-type contact areas. This allows for controlled heat dissipation during reverse bias stress and a more robust module set-up. Especially for cells with enhanced rear dielectric (HIP-MWT III), only little heat dissipation under reverse bias conditions is expected.

4 CONCLUSION

The direct comparison of H-pattern PERC, MWT-BSF and MWT-PERC mc-Si devices clearly demonstrates an advantage in terms of efficiency for the MWT-PERC structure. A cumulated gain in efficiency of up to 1.5 %_{abs} is expected compared to conventional H-pattern cells with aluminium back surface field. The drawback of a significantly increased number of process steps is resolved by the introduction of the simplified HIP-MWT structure. While the complexity of the process sequence is reduced, no negative influence of the simplification on cell efficiency is observed.

The presented peak conversion efficiency of 18.2 % for large-area mc-Si solar cells confirms the high potential of the HIP-MWT structure for industrial fabrication of MWT-PERC-type cells. Laser drilling of the vias forms the only additional process step when going from an H-pattern PERC structure to the HIP-MWT structure, resulting in an increase in cell efficiency of ~0.5 % absolute.

With an enhanced configuration of the rear dielectric, the current density at $V_{rev} = -12$ V is strongly decreased. The median current density J_{rev2} of the improved HIP-MWT III group is even lower than for the non-simplified MWT-PERC reference cells.

Compared to non-simplified MWT-PERC devices, process stability is significantly improved as the rear side does not exhibit structured areas (e.g. emitter areas) except the vias. Therefore, deviations in alignment during contact formation do not necessarily result in shunts or reverse bias instability.

Future experiments will focus on module integration and reverse bias tests after lamination. Additionally, alternative concepts for the formation of the rear diffusion barrier will be evaluated. Especially inkjet printing of silicon oxide based masks is an economically promising approach. Further improvements in efficiency are expected from enhanced front emitter formation and novel metallization technologies [5].

ACKNOWLEDGEMENT

The authors thank all co-workers at the Photovoltaic Technology Evaluation Center (PV-TEC) at Fraunhofer ISE for processing of the samples and gratefully acknowledge the financial support by the German Federal Ministry of Education and Research within the framework of the Leading-Edge Cluster Competition and the research cluster Solarvalley Central Germany under contract No. 03SSF0335I.

REFERENCES

- [1] E. van Kerschaver, R. Einhaus, J. Szlufcik et al., Proceedings of the 2nd World Conference on Photovoltaic Energy Conversion (1998) 1479.
- [2] I.J. Bennett, A. Tjengdrawira, A. Mewe et al., Proceedings of the 24th European Photovoltaic Solar Energy Conference (2009) 3258.
- [3] B. Thaidigsmann, A. Wolf, F. Clement et al., Proceedings of the 25th European Photovoltaic Solar Energy Conference (2010)

- [4] F. Dross, E. van Kerschaver, C. Allebé et al., Proceedings of the 4th World Conference on Photovoltaic Energy Conversion (2006) 1291.
- [5] E. Lohmüller, B. Thaidigsmann, M. Pospischil et al., IEEE Electron Device Letters (2011) accepted for publication.
- [6] B. Thaidigsmann, E. Lohmüller, U. Jäger et al., Physica Status Solidi RRL **5** (2011) 286.
- [7] D. Biro, U. Belledin, A. Weil et al., Proceedings of the 24th European Photovoltaic Solar Energy Conference (2009) 1901.
- [8] E. Schneiderlöchner, R. Preu, R. Lüdemann et al., Proceedings of the 17th European Photovoltaic Solar Energy Conference (2001) 1303.
- [9] S. Mack, D. Scheffler, E.A. Wotke et al., Proceedings of the 26th European Photovoltaic Solar Energy Conference (2011)
- [10] F. Clement, M. Menkoe, D. Erath et al., Solar Energy Materials & Solar Cells **94** (2009) 51.
- [11] D. A. Clugston and P. A. Basore, Proceedings of the 26th IEEE Photovoltaic Specialists Conference (1997) 207.
- [12] B. Thaidigsmann, F. Clement, A. Wolf et al., 1st SiliconPV (2011)
- [13] O. Breitenstein and M. Langenkamp, (Springer Verlag, Berlin/Heidelberg, 2003).